Uncertainty Quantification Study for a Comprehensive Electrostatic MEMS Switch Model

M. Snow[1], A. Bajaj[2]
[1] Purdue University, School of Mechanical Engineering
West Lafayette, IN 47907, United States of America

[2] Purdue University, School of Mechanical Engineering
West Lafayette, IN 47907, United States of America
email: **bajaj@ecn.purdue.edu**

Abstract

This work presents an uncertainty analysis of a comprehensive model for an electrostatic MEMS switch. The goal is to elucidate the effects of parameter variations on certain performance characteristics. A sufficiently detailed model of an electrostatically actuated beam is developed. This model accounts for various physical effects, including the electrostatic fringing field, finite length of electrodes, squeeze film damping, and contact between the beam and the dielectric layer. The performance characteristics of immediate interest are the static and dynamic pull-in voltages for switch. Using Latin Hypercube and other sampling methods, the model is evaluated to find these performances characteristics when variability in the model's geometric and physical parameters is specified. Response surfaces of these results were constructed via Multivariate Adaptive Regression Splines (MARS). Using a Direct Simulation Monte Carlo (DSMC) technique on these response surfaces gives smooth PDF's of the outputs. The relative variation in output due to each input is used to determine the critical parameters.

1 Introduction/Motivation

Micro-ElectroMechanical Systems (MEMS) have shown significant promise as high performance components in RF systems, mass sensors, gyroscopes, accelerometers, and other applications. Among RF MEMS there are switches, filters, mixers and other components [1]. Of these, switches are the most common and the focus of this work. RF MEMS switches offer superior performance to solid-state devices in terms of loss and isolation although being mechanical components means much slower switching speeds compared to silicon devices. This trade off is acceptable in many applications and the hope of better insertion loss and isolation has driven MEMS switch research. Despite creating many designs with good switching characteristics, limited life and early failure has plagued MEMS switches. Although there have been switches that last into the billions and even trillions of cycles, most switches, even those from the same batch don't last nearly this long and many don't work at all. The manufacturing tolerances in MEMS are notoriously poor and additionally the effects that parameters variations have on device behavior are poorly understand. The result is that switch performance and life time are difficult to control or predict. Understanding the effects of these deviations is important for predicting the ranges of performance exhibited by a fabricated design which can vary significantly from the nominal design. Uncertainty Quantification also permits prediction of device yield and is a first step towards predicting switch lifetime.

The system considered in this work is one of the most common structures in RF MEMS. It is a capacitive switch in the form of an electrostatically actuated clamped-clamped beam. In this geometry the RF signal that is to be switched propagates along a coplanar waveguide (CPW). The center conductor of the CPW passes under a flexible beam in a structure that is reminiscent of a free-way overpass. The section of

conductor under the beam is protected by a thin dielectric coating. When there is no DC bias between the conductor and the beam, there exists a gap between the dielectric coating and the bottom of the beam. In this configuration the capacitance of the conductor-beam system is low and as a result a RF signal can propagate freely under the beam. When sufficient DC-bias exists between the beam and the conductor, the oppositely charged conductor and beam experience enough attractive force that the flexible beam will deflect downward and make contact with the dielectric coating. The capacitance in this configuration is typically between 2 and 3 orders of magnitude larger that than in the un-deflected state. For the right range of frequencies this increase in capacitance will appear as an electrical short circuit and the RF signal will not propagate forward but rather be deflected backwards along the CPW. Thus a reflective, capacitive RF switch is created. There are other geometries of switches as well but this geometry remains popular for its relative ease of manufacturing and actuation.

The dynamic process of motion of the switch involves many physical effects including elastodynamics, fluid dynamics, and electromagnetism. The multi-physics nature of this problem can make analysis very difficult and has resulted in significant scientific interest. Additionally, unlike macroscopic systems, where fabrication error in dimensions can be as little as 0.1% in the basic manufacturing equipment such as mills and lathes, micro-scale systems commonly experience geometric deviations up to around 30%. These wide ranges can results in poor device yield and large deviations in performance characteristics. Understanding the effects of these variations is becoming increasingly critical.

This paper is further organized into four main sections: literature review, multi-physics modeling of the switch, methods for uncertainty quantification (UQ methods), and results and discussion. The literature review contains a high-level overview of the multi-physics modeling of MEMS switches, some relevant literature on techniques of uncertainty analysis, and their recent applications in MEMS. Then, the model of a clamped-clamped beam moving in a fluid medium, when actuated by electrostatic forces, is developed. This is followed by a solution methodology in the form of a reduced-order model. The section on UQ methods presents details on the sampling methods used in this work and the response surfaces developed to characterize the uncertainties in predictions of the performance characteristics of the switch. The results section finally gives details of some of the predictions for an example device. The findings of the work are then briefly summarized in the conclusions.

2 Literature Review

The literature on MEMS has become quite extensive. Here we offer a brief review of the literature on MEMS modeling, specifically the mechanical behavior of electrostatically actuated beams, as well some of the UQ efforts in MEMS designs.

2.1 Structural Mechanics

The most basic description of the electrostatically actuated MEMS model is the single degree of freedom approximation. In this model, the mechanical movement of the beam is approximated as that of a lumped mass attached to a spring (see Fig. 1). This basic approach is still useful [2] and is a common educational example of the system at hand as it demonstrates some of the unusual behavior unique to these systems, namely the phenomenon of pull-in. The most basic model of the system in Fig. 1 can be expressed as (assuming no dielectric):

$$M\ddot{x} + Kx = \frac{\epsilon_0 A V^2}{(t_{air} - x)^2} \tag{1}$$

Here, M and K are the mass and linear stiffness of the lumped parameter system, x is the displacement of the mass, t_{air} is the air gap, and t_d is the thickness of the electrode. As the applied voltage is slowly increased, the static deflection of the mass increases and the corresponding gap between the mass element and the dielectric decreases. The biggest stable static solution with the highest corresponding voltage

occurs at $x = \frac{t_{air}}{3}$. The implication of this is that when the voltage of the system is slowly increased, the beam-mass will descend until reaching one third the gap, at which point it will move down rapidly, close the switch and impact the substrate. This sharp transition from up to down state occurs as the linearly increasing restorative force increases with x slower than the rational electrostatic force. This is called pull-in and occurs at the associated pull-in voltage. This is essentially the voltage required to actuate the switch and is a very important performance metric.

Although some of the elements of the simple SDOF model do not hold for a more accurate beam model, the qualitative pull-in behavior remains the same. The beam system under consideration is shown in Fig 2. In this setup it is possible to included realistic models of residual stresses in the beam (which are common in MEMS manufacturing processes) as well as non-linear effects such as beam stretching. This formulation has received attention from many researchers [3, 4]. In this model, the beam is modeled as a thin continuum and the model is typically solved with either a finite element technique or via a reduced order model where the motion of the beam is represented by a linear combination of fundamental mode shapes. The present work uses the latter formulation.

There has also been significant work with fully 3D finite element models [5]. These allow high fidelity modeling of the systems at hand but are encumbered by being computationally expensive.

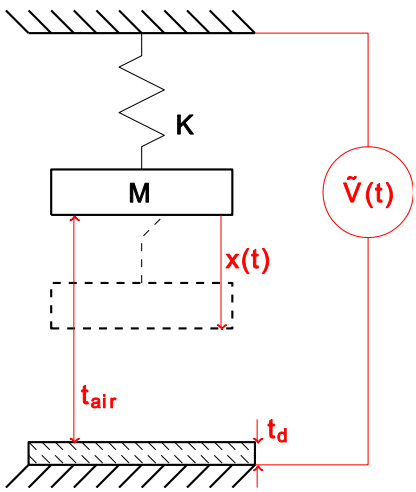

Figure 1. Single-degree-of-freedom equivalent system for a switch

2.2 Electrostatic modeling

The electrostatic force between the beam and the electrode is most commonly represented as the force between a parallel plate capacitor. In the case of the SDOF model the force is expressed as:

$$F_{elec} = \frac{\epsilon_0 V^2(t) A}{2\left(t_{air} + \frac{t_d}{\epsilon_r} - x\right)^2} \tag{2}$$

Almost all 2D models make the assumption that the electric field lines run in the cross section planes of the beam resulting in a similar expression for the electrostatic force.

The parallel plate model is sometimes appropriate but more often than not there is a fringing electrostatic field at the edges of the beam that can contribute non-negligibly to the electrostatic force. There exist many corrections for this fringing field. Many of the result come from earlier works to determine the line-capacitance of micro-strip line wave guides [6] as the geometry is analogous. Other works have focused on creating compact models that correct for the fringing field based on fitting simulations [7] or analytical methods [8]. Some of the more recent models, such as that of Batra et al. [7] are generally accurate to within 2% (as compared to finite element solutions of the electrostatics problem). These corrections still

don't capture the fringing field that is not in the plane of the beam cross section such as fringing field between the edges of the CPW and the bottom of the beam. Also, these devices are commonly manufactured on a silicon substrate which has a very high dielectric constant. The difference in dielectric constant between the substrate and the open gap can significantly distort the electric field.

2.3 Squeeze Film Damping

Damping plays a large role in the dynamic behavior of MEMS devices. It affects switching time, switch bounce, and may also play a large role in determining the lifetime. It is theorized that the repeated contact of a MEMS switch with the substrate causes damage that contributes to failure [9]. The damping force that a switch experiences, especially near contact, affects the speed with which it impacts the substrate.

There are many mechanisms of damping in MEMS, the most prominent of them being the gas damping [1]. The simplest of models for gas damping in MEMS is the linear viscous damping approximation. This model does see use but is a crude approximation when the gap is changing significantly. As the gap becomes small, the squeezing effect becomes very significant. In addition to a damping force, the gas dynamics in MEMS can then contribute other effects including an entrained (added) mass effect due to moving of the gas with the beam [10], and an additional spring force (added stiffness) when the gas is compressed quickly [11].

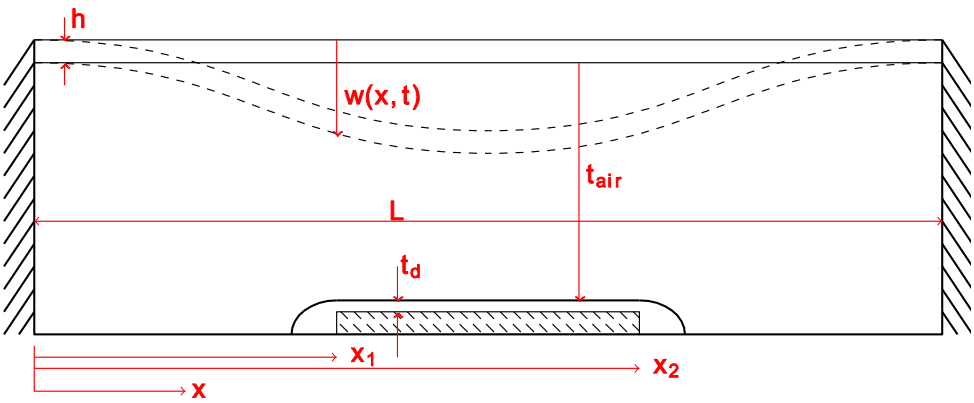

Figure 2. Diagram and nomenclature of beam model for a MEMS switch

2.4 UQ and Probabilistic Design in MEMS

In general, it is recognized that there are two distinct types of uncertainties present in physical models. One type is model uncertainty, also known as 'epistemic' uncertainty. This is the error that exists in the model, that is, how close or far the model is from reality. The other is parameter uncertainty, also known as 'aleatoric' uncertainty. This is associated with the lack of complete knowledge of input parameters, that is, how far they are from nominal and what is the nature of their variability or uncertainty. This work is concerned only with the latter. Given some uncertainty in the model parameters, one needs to understand their effect on the predictions of the model, and this is accomplished by propagating uncertainty through the model, that is, developing the variability in the prediction.

Monte Carlo methods are the most straightforward and easy to implement for developing stochastic description of the output of a simulation model with uncertainty in parameters. These methods are easy to understand, and by definition the results (computed statistics) converge to the correct answer. However, the associated computations become prohibitive as the accuracy of a MC analysis is directly related to the number of samples and accurate models of MEMS devices are often prohibitively expensive from a computational standpoint. To circumvent this difficulty, more advanced methods have been developed. Agarwal and Aluru [12] employed a generalized polynomial chaos (gPC) method to characterize the

variability in pull-in voltage of MEMS. In their work, they successfully used a quadrature sampling approach to find the mean and standard deviation of MEMS performance characteristics like pull-in voltage that matches Monte Carlo analysis results with even with significantly fewer samples. Shanmugavalli et al. used interval analysis to find ranges of static pull-in voltage based on ranges of inputs [13].

Quite distinct from the Monte Carlo and generalized polynomial chaos techniques are the response surface/surrogate model approaches used when the original simulation model is very computationally intensive. Then, the model under consideration is supplanted with a surrogate model, which though non-physical, yields close to correct numerical results within the parameters space at much less computational cost. A sufficient number of samples points from the actual model are needed to construct the response surface. Attempting to construct a surrogate model from insufficient data can lead to erroneous results [14]. Once the surrogate model is created, Monte Carlo analysis on the surrogate model yields output distributions.

Generating samples to create the response surface is a very important part of the uncertainty quantification process and there are a number of ways to do it. Though one can again use the Monte Carlo approach, significant gains are to be had by sampling more intelligently. The ideal sampling is sparse (requiring few model runs), covers the whole input space (so as to not miss any features), is evenly spaced (to avoid redundancy), and non-periodic (to avoid aliasing). While Monte Carlo technique is easy to implement and meets the first and last requirements, it tends towards bunching as well as empty space. The next easiest sampling routine to implement is tensor-grid, wherein the input/parameter space is divided into a rectilinear grid and every grid point is a sample point. When the points are finely spaced, the data looks exactly like the underlying function. This approach becomes computationally prohibitive when one considers higher dimensional problems, e.g., it's rather common for a model under consideration for UQ to have 10 or more inputs, sometimes up to 100 even. Consider a problem with 20 inputs with the input space normalized to a 20-dimensional hypercube. Even if one were to choose a grid spacing of 1, that is, only the corners (which would look hopeless in a 2-d plot) one still requires over a million model evaluations. This is the 'curse of dimensionality' and illustrates the difficulty of intelligently sampling in higher dimensional spaces.

Latin Hypercube (LHS) is one of the most popular sampling methods. Originally proposed by McKay et al. [15], this method consists of dividing the each of the k inputs into s bins and distributing s points such that each bin for each input contains only one point. This is a significant improvement over Monte Carlo sampling but it still isn't full-proof (for example, all of the sample points in a line from one corner of the hypercube to the distant corner satisfies these requirements). There are many improvements to the basic LHS method; optimizing LHS sampling method by some distance criterion [16] and orthogonal arrays which have additional space-filling criterion are two popular options. There are a multitude of other sampling algorithms that have been used successfully. Many of these sampling approaches useful for uncertainty quantification have been implemented in a software toolbox PSUADE (Problem Solving Environment for Uncertainty Analysis and Design Exploration) written at Lawrence Livermore National Laboratories. The PSUADE manual [16] gives a useful summary of these refinements.

2.4.1 Response Surfaces

Given data of the underlying function there is multitude of ways to generate response surfaces. In general it is a good idea to choose a method that is appropriate for the underlying sampling method and model. For example a polynomial response surface would be appropriate for a quadrature rule sampling. Response surfaces should also be fast to evaluate (but not necessarily to create, creation can be intensive) and be able to function with noisy data and outliers. MARS stands for Multivariate Adaptive Regression splines and is the response surface method used in this work. It is discussed in more detail later in the methods section. Again, the PSUADE manual [16] is a good reference for this and other response surfaces methods.

3 Beam (Switch) Modeling

A thorough beam model that incorporates residual stress, non-ideal boundary conditions, non-linear stretching, and corrections for plate-like bending is developed here in a step-by-step process. It also accounts for models for damping, the electrostatic force as well as possible contact with the substrate. The following section covers the use of the Galerkin method to render the resulting PDE into a system of ODEs and the methodology for the solution of these ODE's.

3.1 Structural Dynamics

We begin with the simplest case, that of a straight, unstressed Euler-Bernoulli beam as show in Fig. 2. The equation of motion for free transverse motions of an unstressed, flat Euler-Bernouli beam [17] is given by

$$EI\frac{\partial^4 w}{\partial x^4} + \rho bh\frac{\partial^2 w}{\partial t^2} = 0 \tag{3}$$

This equation reflects only the inertia of the beam and the restorative bending force.

3.1.1 Residual Stresses

Manufacturing processes in MEMS can create significant residual stresses in beam materials. These stresses can manifest as tensile or compressive load and it is important to take them into account as they can significantly influence the dynamics of the beam. Incorporating axial stress brings in a second derivative term [17] making the beam equation

$$EI\frac{\partial^4 w}{\partial x^4} - N\frac{\partial^2 w}{\partial x^2} + \rho bh\frac{\partial^2 w}{\partial t^2} = 0 \tag{4}$$

3.1.2 Stretching

The axial stress in the beam is really a combination of the residual stress, which exists in the rest state, and axial stress due to stretching or compression of the beam. Beam stretching introduces additional axial load dependent on the deflection of the beam and is the first non-linear element to the model. The incorporation of the stretching requires an approximation of the changes in the arc-length of the beam. The EOM with stretching can be expressed as [3]

$$EI\frac{\partial^4 w}{\partial x^4} - \left[\frac{EA}{2L}\int_0^L \left(\left(\frac{\partial w}{\partial x}\right)^2\right)dx + N\right]\left(\frac{\partial^2 w}{\partial x^2}\right) + \rho bh\frac{\partial^2 w}{\partial t^2} = 0 \tag{5}$$

3.1.3 Plate Stiffness Correction

When a beam is very wide relative to its thickness, the bending stiffness is slightly more than EI due to Poisson's ratio effects. We adopt a correction for plate-like behavior in form of an effective Young's modulus:

$$\begin{aligned} E_{ef} &= \frac{1}{1-\nu^2}E \qquad && \{b > 5h\} \\ E_{ef} &= E && \{b < 5h\} \end{aligned} \tag{6}$$

This effective Young's modulus is used in place of E for the rest of the calculations.

Obviously, this discontinuity in bending stiffness results in some inaccuracies. In fact, the effective bending stiffness of a beam as its dimensions transit to those of a plate is a complicated problem that depends on more than the width-to-thickness ratio and does not have a simple answer [18]. As such we will accepts the errors from this approximation and keep it for its simplicity.

3.1.4 Boundary Conditions

MEMS beam anchors can never be truly rigid. In certain geometries and manufacturing methods, the fixed boundary condition can be completely justifiable but in other conditions it may differ from reality significantly. The pinned support with torsion-spring boundary condition is therefore more appropriate than the clamped boundary condition. Using the torsion-spring boundary condition with a large spring constant effectively covers the truly fixed condition and in the limit when the spring constant goes to zero the end condition approximates a pinned end condition. The pinned support with torsion-spring boundary condition can be expressed as

$$\begin{gathered} w(0,t) = 0 \quad w(L,t) = 0 \\ w''(0,t) = k_t w'(0,t) \quad w''(L,t) - k_t w'(0,t) \end{gathered} \tag{7}$$

where k_t is the spring constant of the torsion spring.

3.1.5 Electrostatic Forces

The parallel-plate electrostatic force model was already introduced in equation (1), where the force is attractive. The accuracy of the parallel-plate assumption is directly related to width of the beam with a wider beam better approximating a parallel plate. For a narrower beam, a significant portion of its electric field emanates from its sides and top, making a parallel plate model inappropriate. There are numerous corrections to the parallel-plate model to account for the fringing field. Batra et al. [7] modeled the capacitance of a narrow microbeam with a modifying factor to the basic parallel-plate model. This model of Batra et al. was chosen for its wide range of applicability. In this model [7], the electrostatic force per unit length can be expressed as

$$F_{elec} = \frac{\epsilon_0 b V^2(t)}{2\left(t_{air} + \frac{t_d}{\epsilon_r} - x\right)^2}\left(1 + 0.24 A_0 \left(t_{air} + \frac{t_d}{\epsilon_r} - x\right)^{0.76}\right) \tag{8}$$

where

$$A_0 = 0.85\frac{1}{b^{0.76}} + 2.5\frac{h^{0.26}}{b} \tag{9}$$

3.1.6 Finite Electrodes

Many models assume the electrode and the beam to completely overlap, though this often does not reflect reality. More frequently, the electrode is in the form of a micro-strip that only exists under a portion of the beam. It is important to realize that in this case, there exists fringing field along the whole perimeter of the rectangular area of overlap between the beam and the electrode. The model above accounts only for the fringing field between the sides of the beam and the top of the electrode, and not between the sides of the electrode and the bottom of the beam. If the electrode exists under the beam from $x = x_1$ to $x = x_2$ as in Fig. 2, the electrostatic force can be expressed as

$$F_{elec} = \frac{\epsilon_0 b V^2(t)}{2\left(t_{air} + \frac{t_d}{\epsilon_r} - x\right)^2}\left(1 + 0.24A_0\left(t_{air} + \frac{t_d}{\epsilon_r} - x\right)^{0.76}\right) * (H(x - x_1) - H(x - x_2)) \tag{10}$$

where $H(x - a)$ is the Heaviside step function at $x = a$. Note that this does not account for the fringing field between the sides of the electrode and the bottom of the beam. It is possible to further refine the model by making x_1 and x_2 into effective end points that vary with the instantaneous geometry of the system, thereby more closely mimicking the true fringing field, though this is not done in present study.

3.1.7 Damping Force

Fluid damping is arguably the most difficult aspect of MEMS modeling and there is currently not a compact damping model in literature that incorporates the squeezing, gas rarefaction and surface effects required to accurately model a MEMS switch closing. Two damping models were considered for inclusion, the basic viscous damping model and the compact squeeze film damping model by Guo and Alexeenko [19].

In the basic linear viscous damping model, the damping force per unit length is expressed as:

$$F_{damp} = c\dot{w} \tag{11}$$

This model is very easy to implement but is a poor approximation of the actual physics. In reality, the increased damping at smaller gaps is very significant, and thus the use of the other damping model (due to Guo and Alexeenko [19]). They modeled the squeeze film effect as a linear viscous damping where the coefficient of damping varies with the beam displacement. Thus,

$$F_{damp} = c(w)\dot{w} \tag{12}$$

The damping coefficient is derived by fitting a rational function to results of rarefied gas simulations for beams oscillating with small amplitudes at various rarefactions (as specified by Knudsen number):

$$c(w) = \frac{10.39\left(\frac{b}{t_{air} - w}\right)^{3.1}}{1 + 1.374\left(\frac{b}{t_{air} - w}\right)^{1.825}\left(\frac{\lambda}{b}\right)^{0.966}} \tag{13}$$

Note that the model is a velocity proportional damping model where the damping coefficient depends on the gap-separation. Thus, the damping force is really a nonlinear function of beam displacement and velocity. It should be noted that the damping force approaches infinity as the beam approaches contact. This is clearly non-physical as contact and bouncing are observed experimentally. A simple correction of changing t_{air} in equation (13) to $t_{air} + 40nm$ to represent the effects of surface roughness was used to eliminate this singularity. Although it does give nice results, it should be noted that this correction hasn't been verified against other data or models.

3.1.8 Impact Modeling

A soft-impact contact model is employed here. The impacted substrate acts as a stiff, distributed spring and thus the contact force term in the equation of motion is defined as:

$$F_{contact} = -\frac{E_f b}{t_d}(w - t_{air})(w \geq t_{air}) \tag{14}$$

It should be noted that the impact will occur before the singularity in the electrostatic force. Also, as we have defined the attraction of the beam to the electrode as the positive direction, and hence the minus sign in the contact force expression. For the static case, the compression of the dielectric by charges on either side results in the above stiffness. For the dynamic case, when the beam impacts the dielectric, the

substrate is not truly rigid and finding a reasonable approximation to the stiffness is difficult. This is a simple model that provides qualitative correct result, but it does not include surface roughness, adhesion or any of the more complicated surface effects that are relevant at the microscale. As it turns out, this stiffness is so high that it makes results computed by varying the contact stiffness over orders of magnitude indistinguishable. From a computational standpoint lower stiffness are preferable as they make the calculations more numerically stable.

3.2 Complete Equation of Motion for the Switch

After incorporating all of the above effects and their respective sub-models, we arrive at the general equation of motion for a switch:

$$\rho A\ddot{w} + EIw^{IV} + c(w)\dot{w} - \left[\frac{EA}{2L}\int_1^0 w'^2 dx + N\right] w'' = \frac{\epsilon_0 b V^2(t)}{2\left(t_{air} + \frac{t_d}{\epsilon_r} - w\right)^2}\left(1 + 0.24A_0\left(t_{air} + \frac{t_d}{\epsilon_r} - w\right)^{0.76}\right) * \left(H(x - x_1) - H(x - x_2)\right) - \frac{E_f b}{t_{air}}(w - t_{air})(w \geq t_{air}) \tag{15}$$

where c(w) is the appropriate correction for squeeze film damping. The next step is to make equation (15) more convenient by non-dimensionalizing it with the follow non-dimensional parameters;

$$\hat{x} = \frac{x}{L} \quad \hat{t} = \frac{t}{T} \quad \widehat{w} = \frac{w}{t_{air} + \frac{t_d}{\epsilon_r}} \quad \hat{x}_1 = \frac{x_1}{L} \quad \hat{x}_2 = \frac{x_2}{L} \tag{16}$$

The end result of this is the non-dimensionalized equation of motion is

$$\widehat{w}^{IV} + \ddot{\widehat{w}} + c(w)\dot{\widehat{w}} = \alpha_1\left[\int_0^1 w'^2 dx + N\right] w'' + \frac{\alpha_2 V^2(t)}{(1 - \widehat{w})^2}(1 + A_1(1 - \widehat{w})^{0.76})\left(H(\hat{x} - \hat{x}_1) - H(\hat{x} - \hat{x}_2)\right) + \alpha_3\left(\widehat{w} \geq \frac{t_{air}}{t_{air} + \frac{t_d}{\epsilon_r}}\right)\left(\widehat{w} - \frac{t_{air}}{t_{air} + \frac{t_d}{\epsilon_r}}\right) \tag{17}$$

where

$$\alpha_1 = 6\left(\frac{t_{air} + \frac{t_d}{\epsilon_r}}{h}\right)^2 \qquad \alpha_2 = \frac{6\epsilon_0 L^2}{Eh^3\left(t_{air} + \frac{t_d}{\epsilon_r}\right)^3}$$

$$\alpha_3 = \frac{E_f L^4 b}{t_d EI} \qquad T = \sqrt{\frac{\rho b h L^4}{EI}} \qquad c(w) = \frac{\hat{c}(w)L^4}{EIT} \qquad \widehat{N} = \frac{NL^2}{EI} \tag{18}$$

$$A_1 = 0.24A_0\left(t_{air} + \frac{t_d}{\epsilon_r}\right)^{0.76}$$

Hats are dropped from this point forward for convenience.

3.3 Solution Methodology

In order to solve the beam model in equation (17), it is assumed that the solution can be approximated at any given time by a linear combination of the first M linear mode-shapes of the undamped and unforced microbeam. The solution then takes the form

$$w(x,t) = \sum_{i=1}^{M} u_i(t)\phi_i(x) \tag{19}$$

As M becomes larger, the approximation and thus the solutions become more accurate. However, as we will see, the convergence for the performance variables of static and dynamic pull-in voltage can be quite fast. The mode-shapes are also normalized to obey the orthogonality property

$$\int_0^1 \phi_i \phi_j dx = \delta_{ij} \tag{20}$$

where ϕ_i is the i-th linear undamped mode of the beam with appropriate boundary conditions and u_i are time varying coefficients. The mode shapes are the solutions to the equation:

$$\phi_i^{iv} = N\phi_i'' + \omega_i^2 \phi_i \tag{21}$$

The boundary conditions for a fixed-fixed beam are the same as in the dimensional case.

There exist closed-form expressions for the modal frequency equations and mode-shapes. The formulas for a cantilever beam can be found in Rao [17] and many other sources. The closed-form expressions for a fixed-fixed beam under axial tension can be found in Shaker [20]. The derivation of the mode shapes and frequency equations for a beam under tensile load with pinned ends and torsion spring conditions is given in an appendix of the first author's thesis [21].

3.3.1 Reduced Order Method

We now apply the modal expansion by substituting equations (19) and (21) into equation (17). Multiplying the resulting expression by ϕ_n and integrating from 0 to 1 yield the system of ODE's for the modal amplitudes. The orthogonality condition in equation (20) results in simplifications of the inertia, bending stiffness, residual stress and stretching terms. As for the remaining terms, w has been left as is rather than the modal sum form of equation (19), although the equivalence remains. The final equations are:

$$\begin{aligned} \ddot{u}_n + \omega_n^2 u_n = &\int_0^1 c(w)\dot{w}\phi_n dx \\ &+ \alpha_1 \sum_{i,j,k=1}^{M} u_i u_j u_k \int_0^1 \phi_i' \phi_j' dx \int_0^1 \phi_k'' \phi_n dx \\ &+ \alpha_2 V^2(t) \int_{x_1}^{x_2} \left(\frac{1}{(1-w)^2} + A_1 \frac{1}{(1-w)^{1.24}} \right) dx \\ &+ \alpha_3 \int_0^1 (w - t_{air})(w \geq t_{air}) dx \end{aligned} \tag{22}$$

where $n = 1,2,\ldots,M$.

Considering equations (22) we can see that the system contains at most third-order terms. The integrals in the summation terms do not vary with time and as such they may be used from a table when performing calculations. This is not the case with the other integrals. When integrating equations (22), w must be reassembled at every time step using the modal summation in equation (19), likewise the integral terms depending on w must be computed at every time step. The main drawback of this formulation is the requirement to perform several space integrations at every time step. There are methods to avoid this

problem [3, 21] but they result in other inconveniences such as non-diagonal mass matrices, higher-order terms and difficult in representing non-linear effects such as squeeze film damping, fringing field and contact conditions.

3.4 Model Verification

Some deterministic results are presented in Table 1 where the static pull-in voltages computed by the above model are compared to results available in the literature. The static pull-in voltage was already explained before and it is computed by finding static solution of the model. The parameters are: $L = 250\mu\text{m}$, $b = 50\mu\text{m}$, $h = 3\mu\text{m}$, $t_{air} = 1\mu\text{m}$, $t_d = 0\mu\text{m}$, $x_1 = 0$, $x_2 = 1$, $E = 169\text{GPa}$, $\nu = 0.06$, and $k_t = 0$.

σ (MPa) (residual stress)	0	100	-25
V(MEMCAD)[22]	39.13	57.62	39.63
V [23]	40.10	57.60	33.60
V This model	39.21	57.75	32.79

Table 1. Comparison of Static Pull-in Voltages predicted by different models.

4 Uncertainty Quantification

Using the model above, we now characterize the effects of input parameter variations on system performance. Often in MEMS manufacturing processes, multiple features are made in the same processing step, and as such, some covariance in the parameter distributions is expected. To allow for this in our analysis we have restricted the parameter variations to have normal distributions. For a UQ analysis, we have defined two quantities of interest as the performance measures. Now, we need to choose the number inputs to be varied. It is possible, and most informative to perform the analysis with all parameters allowed to vary. However this can be rather time consuming when the system depends on 20+ parameters. Often only the behavior and interactions of a few parameters are of interest and the rest can be left to their nominal values. Next, using an appropriate sampling algorithm, a few hundred data points are computed from the model. From these sample points, a function is created that closely approximates the actual predictions of the model. This function, the 'response surface' is then used as a surrogate for the actual model. Monte Carlo sampling can then be used on these response surfaces to find the PDF's of outputs and the mathematical form of the response surfaces can be used to discern the relative important of the parameter variations.

4.1 Defining Output Parameters of Interest

In our UQ problem we first define the performance measures of interest. For this work, we have chosen the static pull-in voltage and the dynamic pull-in voltage as the predictions of interest.

The 'Static Pull-in' voltage is defined as the highest voltage at which there exists at least one equilibrium solution to the system not involving contact. At a voltage any higher than this, the beam will pull-in and make contact. The static pull-in voltage was found by first finding all of the pre-contact static solutions of the beam model. The static solutions were found via an enforced displacement scheme. In this scheme a specified (chosen) point on the beam is forced to have a given displacement. To find the static solutions that passes through this point (and there always is one, assuming no buckling and a continuous actuation electrode), a Newton-Raphson scheme was used. The highest voltage associated with one of these pre-contact static solutions is returned as the pull-in voltage. Details of the algorithm are given in [21].

A ‘Dynamic Pull-in’ voltage is defined as the amplitude of a step voltage applied to the system that causes it to close. This voltage is smaller than the static pull-in voltage due to dynamic effects [4] typically by 8% or so, but this can vary based on switch geometry. The dynamic pull-in voltage is found via a bisection search method [21]. Initially, guesses are used to establish upper and lower bounds on the voltage where the beam does, and doesn’t pull-in, respectively. Knowing that the actual voltage lies in this voltage interval, the interval is iteratively divided in two until sufficiently small. The system is integrated with a step voltage that is in the middle of this interval. Depending on the outcome of this integration, the upper or lower half of the previous interval becomes the new interval and the process repeated until the dynamic pull-in voltage is known to within a certain threshold, 10mV for example.

4.2 Sampling Methods

For the response surface generation, two sampling methods were used. The first one was the straight forward Latin Hypercube sampling [15]. The second was an improved space filling design. The space filling design consists of randomly seeding the parameter space with points and then evolving those points via a repulsive $1/r^2$ model among the k-nearest neighbors. If k is set to be all of the sample points, this is analogous to charges on a hypercube, and all of the points will migrate to the surface of the sample space. If k is set to roughly the dimension of the parameter space, the sampling will settle into some equilibrium. The result is analogous to a crystallization process, with periodic space-filling structure appearing. Periodicity isn’t something that is desired in sampling routines. To eliminate this, 10-15% of the sample points were set as stationary. This results in significantly reduced periodicity. This sampling routine is discussed in more detail in [21].

The sampling routine used on the response surface is Monte Carlo. The extremely fast evaluation times of the response surface functions made this feasible. It is also easy to implement covariance with normally distributed Monte Carlo points.

4.3 Response Surface Generation

The technique used in this work to generate response surfaces is MARS [24] which has been implemented in PSUADE [16]. MARS stands for Multi-variate Adaptive Regression Splines. The MARS technique was originally proposed by Friedman [24]. The technique consists of local regressions matched at their boundaries with ‘knot-functions’. The model is built in 2 passes. In forward pass, localized basis functions are added, progressively lowering the mean-squared error. In the backwards pass, localized basis functions that contribute the least to error minimizations are removed. This backwards pass reduces over-fitting of the model. The results presented here have been computed with AREAlab [25], a MATLAB implementation of MARS. Results have also been computed with PSUADE [16].

4.4 UQ –example

We subject a switch model similar to the one considered in section 3.4 to the uncertainty analysis. A fixed-fixed beam geometry is assumed, and the nominal parameters that may exhibit variability as well as

	$L(\mu)$	$b(\mu)$	$h(\mu)$	$t_{air}(\mu)$	$E(GPa)$	$\sigma(MPa)$
Nominal	250	50	3	1	169	0
Std.	1.5	.5	.25	.08	6	5

Table 2. Nominal inputs and standard deviations for the switch parameters.

their standard deviations assumed are given in Table 2. Thus, there are six input parameters. The non-varying parameters are assumed to be: dielectric thickness, electrode extent, beam material density, dielectric constant, and the Poisson ratio. Their values are $t_d = 0.2\mu, x_1 = 0.4L, x_2 = 0.6L, \rho = 2300kgm^{-3}, \epsilon_r = 3, \nu = 0.06$. The response surfaces for this example were generated from 600 sample points. K-fold cross-validation resulted in an averaged R^2 of greater than 0.999 in both cases.

Given this data, we would like to know the variability in the model predictions of interest, static and dynamic pull-in voltages. Using the methods discussed previously, a sample of (500) points was taken of the +/- 4 standard deviations input space. A response surface of pull-in data was generated with the MARS algorithm using the ARESlab toolbox. To find a smooth PDF of pull-in voltages, 1e6 Monte Carlo samples were generated using the statistics in Table 2. A histogram of the results is given in Fig. 3.

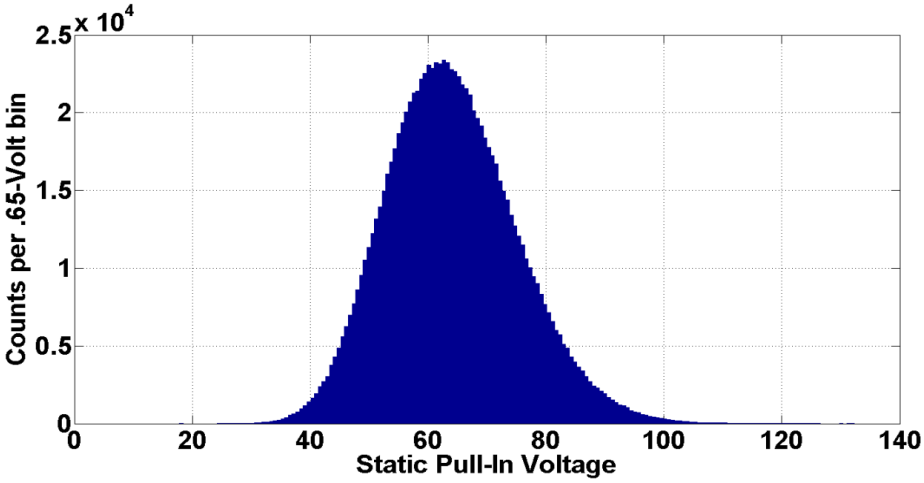

Figure 3. Histogram of Static Pull-in Voltages: nominal= 64.09V, mean =64.05V, Std. =11.07V

A similar analysis was performed for the dynamic pull-in voltage. It is important to realize that not every switch realization is going to close at all. Assuming an actual actuation voltage of 1.3 times the nominal static pull-in voltage, some switches may not pull-in at all. A histogram of dynamic pull-in voltages given in Fig. 4 shows that 1.97% of switches in this case would fail to pull-in at all. This is better than the 5.00% percent that would be predicted if static pull-in voltage was used instead of dynamic pull-in voltage.

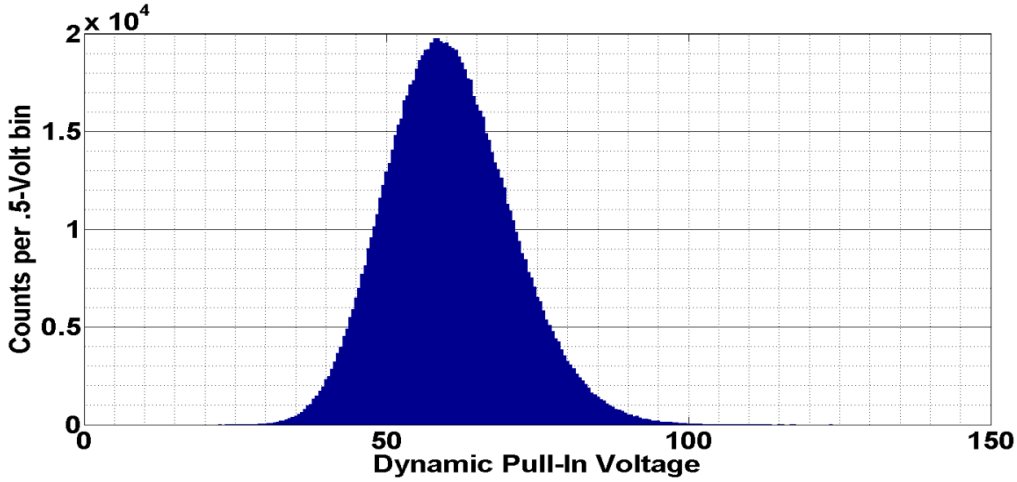

Figure 4. Histogram of Dynamic Pull-In Voltages: nominal= 60.18V, mean =60.49V, Std. =10.26V

4.4.1 Critical Parameter Identification

It is also important to identify the critical parameters for the system, that is, the parameters that significantly influence the outputs of the model. Here, critical parameters are identified by their sensitivities, taken at the nominal configuration, weighted by their standard deviations. The sensitivities are found by taking partial derivatives of the surrogate function and multiplying those partial derivatives by the ranges given for the parameters. This then represents a local sensitivity analysis of the model. These numbers are normalized to sum to one and thus we can express as the percent of variation due to certain parameters. Obviously, this does not capture effects such as strong self-interactions or interactions with other variables but it does give a picture of the parameters that drive the problems at the first-order. This data is presented in Table 3.

	L	b	h	t_{air}	E	σ
Static Pull-in	0.0381	0	0.408	0.390	0.059	0.103
Dynamic Pull-in	0.0378	0	0.422	0.390	0.058	0.094

Table 3. Normalized, weighted sensitivities of the pull-in voltages for a switch.

5 Conclusion

A thorough model of an electrostatically actuated MEMS beam was presented. Distributions of output parameters were determined via a response surface approach. Static and dynamic pull-in distributions were derived. Using the dynamic pull-in voltage distributions, the yield of switches that would actuate under 1.3 times the nominal static pull-in voltage was determined. The most critical parameters were found to be the switch thickness and air gap height. This is because the system is very sensitive to these dimensions and vertical dimensions are typically among the most difficult to control.

Acknowledgements

This work was supported by the National Nuclear Security Administration under the Center for Prediction of Reliability, Integrity and Survivability of Microsystems (PRISM).

References

[1] G. M. Rebeiz, *RF MEMS: Theory, Design, and Technology*. New York, NY, USA: John Wiley & Sons, Inc., (2003).

[2] R. P. LaRose, K. D. Murphy, *Impact dynamics of mems switches*, Nonlinear Dynamics, Vol. 60, (2010), pp. 327–399.

[3] M. Younis, E. Abdel-Rahman, A. Nayfeh, *A reduced-order model for electrically actuated microbeam-based mems*, Journal of Microelectromechanical Systems, Vol. 12, No. 5, (2003), pp. 672–680.

[4] P. C.-P. Chao, C. W. Chiu, T.-H. Liu, *DC dynamic pull-in predictions for a generalized clamped-clamped micro-beam based on a continuous model and bifurcation analysis*, Journal of Micromechanics and Microengineering, Vol. 18, No. 11, (2008), p. 115008 (14pp).

[5] B. McCarthy, G. Adams, N. McGruer, D. Potter, *A dynamic model, including contact bounce, of an electrostatically actuated microswitch*, Journal of Microelectromechanical Systems, Vol. 11, No. 3, (2002), pp. 276 –283.

[6] N. Meijs, J. Fokkema, *VLSI circuit reconstruction from mask topology*, Integration, Vol. 2, No. 2, (1984), pp. 363–366.

[7] R. Batra, M. Porfiri, D. Spinello, *Electromechanical model of electrically actuated narrow microbeams*, Journal of Microelectromechanical Systems, Vol. 15, No. 5, (2006), pp. 1175–1189.

[8] W. H. Chang, *Analytical IC metal-line capacitance formulas* (Short Papers), IEEE Transactions on Microwave Theory Techniques, Vol. 24, (1976), pp. 608–611.

[9] S. Mariani, A. Ghisi, A. Corigliano, S. Zerbini, *Modeling impact-induced failure of polysilicon mems: A multi-scale approach*, Sensors, Vol. 9, No. 1, (2009), pp. 556-567.

[10] J. F. Vignola, J. A. Judge, J. Jarzynski, M. Zalalutdinov, B. H. Houston, J. W. Baldwin, *Effect of viscous loss on mechanical resonators designed for mass detection*, Applied Physics Letters, Vol. 88, No. 4, (2006), p. 041921.

[11] M. Bao, H. Yang, *Squeeze film air damping in mems*, Sensors and Actuators A: Physical, Vol. 136, No. 1, (2007), pp. 3 – 27, 25th Anniversary of Sensors and Actuators A: Physical.

[12] N. Agarwal, N. Aluru, *Stochastic modeling of coupled electromechanical interaction for uncertainty quantification in electrostatically actuated mems*, Computer Methods in Applied Mechanics and Engineering, Vol. 197, No. 43-44, (2008), pp. 3456–3471.

[13] M. Shanmugavalli, G. Uma, B. Vasuki, M. Umapathy, *Design and simulation of mems devices using interval analysis*, Journal of Physics: Conference Series, Vol. 34, No. 1, (2006), p. 601.

[14] A. A. Giunta, J. M. McFarland, L. P. Swiler, M. S. Eldred, *The promise and peril of uncertainty quantification using response surface approximations*, Structure and Infrastructure Engineering: Maintenance, Management, Life-Cycle Design and Performance, Vol. 2,(2006), pp. 175–189.

[15] M. D. McKay, R. J. Beckman, W. J. Conover, *A comparison of three methods for selecting values of input variables in the analysis of output from a computer code*, Technometrics, Vol. 21, (1979), pp. 239–245.

[16] C. Tong, *PSAUDE User's Manual*, 1st ed., Center for Applied Scientific Computing Lawrence Livermore National Laboratory, Livermore, CA 94551-0808, (May 2009).

[17] S. Rao, *Mechanical Vibration 4th ed.* Pearson Prentice Hall, (2003).

[18] S. K. Kaldor, I. C. Noyan, *Differentiating between elastically bent rectangular beams and plates*, Applied Physics Letters, Vol. 80, No. 13, (2002), p. 2284.

[19] X. Guo, A. Alexeenko, *Compact model of squeeze-film damping based on rarefied flow simulations*, Journal of Micromechanics and Microengineering, Vol. 19, No. 4, (2009), p. 045026 (7pp).

[20] F. Shaker, *Effect of axial load on mode shapes and frequencies of beams*, Lewis Research Center Report *NASA-TN-8109*, Technical Report, (Dec. 1975).

[21] M. G. Snow, *Comprehensive Modeling of Electrostatically Actuated MEMS Beams including Uncertainty Quantification*, Master's Thesis, Purdue University, (2010) (in progress).

[22] P. M. Osterberg, S. D. Senturia, *M-test: A test chip for mems material property measurement using electrostatically actuated test structures*, Journal of Microelectromechanical Systems, Vol. 6, (1997), pp. 107–118.

[23] H. Sadeghian, G. Rezazadeh, P. Osterberg, *Application of the generalized differential quadrature method to the study of pull-in phenomena of mems switches*, Journal of Microelectromechanical Systems, Vol. 16, No. 6, (2007), pp. 1334–1340.

[24] J. H. Friedman, *Multivariate adaptive regression splines*, Annals of Applied Statistics, Vol. 19, (1991), pp. 1–67.

[25] G. Jekabsons. *Areslab: Adaptive regression splines toolbox for matlab*, (2009). [Online]. Available: http://www.cs.rtu.lv/jekabsons/.